

# Nanoscale

rsc.li/nanoscale



ISSN 2040-3372



PAPER






Miroslav Medved<sup>†</sup>, Michal Otyepka *et al.*

Reactivity of fluorographene is triggered by point defects: beyond the perfect 2D world



Cite this: *Nanoscale*, 2018, 10, 4696

# Reactivity of fluorographene is triggered by point defects: beyond the perfect 2D world†

Miroslav Medved', \*<sup>a</sup> Giorgio Zoppellaro, <sup>a</sup> Juri Ugolotti,<sup>a</sup> Dagmar Matochová,<sup>a</sup> Petr Lazar,<sup>a</sup> Tomáš Pospíšil,<sup>b</sup> Aristides Bakandritsos,<sup>a</sup> Jiří Tuček, <sup>a</sup> Radek Zbořil <sup>a</sup> and Michal Otyepka \*<sup>a</sup>

Preparation of graphene derivatives using fluorographene (FG) as a precursor has become a key strategy for the large-scale synthesis of new 2-D materials (e.g. graphene acid, cyanographene, allyl-graphene) with tailored physicochemical properties. However, to gain full control over the derivatization process, it is essential to understand the reaction mechanisms and accompanying processes that affect the composition and structure of the final products. Despite the strength of C–F bonds and high chemical stability of perfluorinated hydrocarbons, FG is surprisingly susceptible to reactions under ambient conditions. There is clear evidence that nucleophilic substitution on FG is accompanied by spontaneous defluorination, and solvent-induced defluorination can occur even in the absence of any nucleophilic agent. Here, we show that distributed radical centers (fluorine vacancies) on the FG surface need to be taken into account in order to rationalize the defluorination mechanism. Depending on the environment, these radical centers can react as electron acceptors, electrophilic sites and/or cause homolytic bond cleavages. We also propose a new radical mechanism of FG defluorination in the presence of *N,N'*-dimethylformamide (DMF) solvent. Spin-trap experiments as well as <sup>19</sup>F NMR measurements unambiguously confirmed formation of *N,N'*-dimethylformyl radicals and also showed that *N,N'*-dimethylcarbonyl fluoride plays a key role in the proposed mechanism. These findings imply that point defects in 2D materials should be considered as key factor determining their chemical properties and reactivity.

Received 18th December 2017,  
Accepted 6th February 2018

DOI: 10.1039/c7nr09426d

rsc.li/nanoscale

## 1. Introduction

The discovery of graphene<sup>1</sup> in 2004 opened a route to a new class of carbon-based 2D materials with unique chemical, electronic and magnetic properties. Whereas graphene itself is chemically a low reactive semimetal with high electron conductivity, even dilute concentrations of chemisorbed impurities can dramatically change its band structure and induce local magnetic moments.<sup>2</sup> Increasing the adsorbate concentration can further disrupt the  $\pi$ -conjugated network, transforming the conducting material to an insulator through a variety of intermediate states.<sup>3,4</sup> Possibilities for tuning the band gap characteristics and associated electronic and mag-

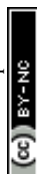
netic properties by graphene derivatization provide an auspicious base for future technological advancements, including development of batteries,<sup>5–7</sup> biosensing,<sup>8</sup> gas sensing on surfaces<sup>9</sup> and solar cell technologies.<sup>10</sup> Nevertheless, selective and controllable covalent graphene functionalization remains a challenging task due to the limited reactivity of graphene.<sup>11,12</sup> Many proposed direct derivatization strategies suffer from a low degree of functionalization<sup>13–16</sup> or require harsh reaction conditions that strongly affect the final stoichiometry and chemical structure of the resulting graphene derivative.<sup>17,18</sup>

Fluorographene (FG)<sup>19–21</sup> offers a promising alternative for graphene derivatization because (i) chemisorption of monovalent fluorine atoms prevents formation of complex (non-stoichiometric) structures; (ii) the material is thermally stable up to 400 K; (iii) the pristine 3D material, graphite fluoride, is available in large-scale as an industrial lubricant; and (iv) FG reacts readily as an electrophile under mild conditions.<sup>22–26</sup> Owing to these features, FG has recently been used as a precursor for the synthesis of several graphene derivatives, including amino-graphenes,<sup>26–30</sup> cyanographene,<sup>31</sup> carboxygraphene (graphene acid),<sup>31</sup> sulfur-linked derivatives<sup>25,32</sup> and alkylated graphenes.<sup>33</sup> During the chemical transformation of FG, substitution of fluorine atoms proceeds simultaneously with

<sup>a</sup>Regional Centre of Advanced Technologies and Materials, Department of Physical Chemistry, Faculty of Science, Palacký University in Olomouc, 17. listopadu 1192/12, 771 46 Olomouc, Czech Republic. E-mail: Miroslav.Medved@upol.cz, Michal.Otyepka@upol.cz

<sup>b</sup>Centre of the Region Haná for Biotechnological and Agricultural Research, Department of Chemical Biology and Genetics, Faculty of Science, Palacký University in Olomouc, 17. listopadu 1192/12, 771 46 Olomouc, Czech Republic

†Electronic supplementary information (ESI) available. See DOI: 10.1039/c7nr09426d





Nanoscale, 2018, 10, 4696–4707 | 4697

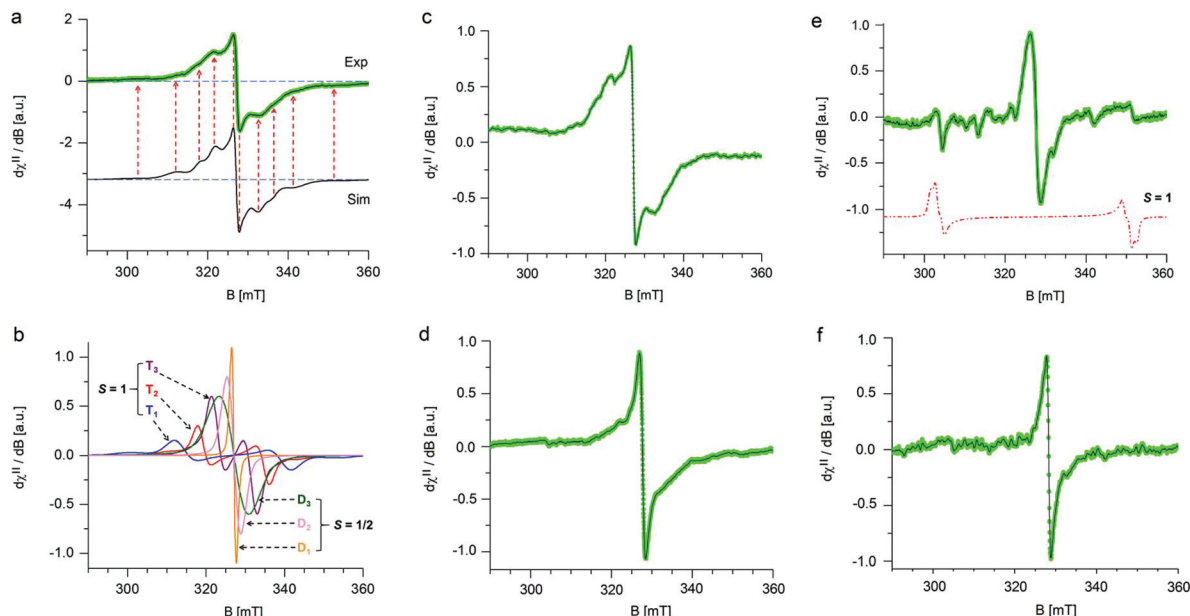


**Fig. 1** Low temperature ( $T = 123$  K) frozen matrix X-band EPR spectra of GrF dispersed in benzene or DMF recorded at various times. (a) GrF freshly dispersed in benzene (green line, Exp) and its EPR simulation (black line, Sim). (b) Overview of the diverse spin components encoded in the EPR envelope shown in (a, Sim); the labels  $T_1$ ,  $T_2$  and  $T_3$  indicate triplet ( $S = 1$ ) species, whereas  $D_1$ ,  $D_2$  and  $D_3$  indicate doublet ( $S = 1/2$ ) species. The relative weights were as follows:  $T_1$  (4.3%),  $T_2$  (8.4%),  $T_3$  (16.9%),  $D_1$  (31.0%),  $D_2$  (22.5%),  $D_3$  (16.9%). (c) GrF freshly dispersed in DMF. (d) GrF/DMF solution after 6 h. (e) GrF/DMF solution after 7 days. (f) GrF/DMF solution after 10 days. Experimental parameters: 9.14–9.16 GHz frequency, 100 kHz modulation frequency, 30 ms time constant, 0.5–0.8 mT modulation width, 0.4–0.6 mW applied microwave power. In (a) and (c–f), the solid black line corresponds to the resolution enhanced EPR resonance line (Savitzky–Golay, denoise algorithm).

nance line of the system in benzene was rather broad ( $\sim 30$  mT field-spread), it exhibited several small resonances that developed symmetrically with respect to an intense narrow central line, a signature of overlapped contributions of triplet and doublet spin-states. The observed  $g$ -averaged ( $g_{\text{avg}}$ ) value was estimated to be 2.000 and validated by recording the spectrum together with the  $\text{Mn(II)MgO}$  standard (JEOL internal reference standard,  $\text{Mn(II)}$ ,  $g_{\text{eff}} = 2.00101 \pm 0.00005$ , ESI, Fig. S5 and S6†). A comparable EPR spectrum was observed for the neat GrF powder (ESI, Fig. S1a and S3†). Similar EPR spectra have been previously reported around the  $g = 2$  region ( $\sim 280$ – $380$  mT) by Panich and co-authors<sup>41</sup> on polycrystalline graphite fluoride ( $\text{CF}_n$ ) obtained by fluorination of petroleum coke as well as by Giraudet and co-authors in a later report ( $\sim 310$ – $380$  mT region).<sup>42</sup> However, we noticed that by recording the EPR signal of the GrF powder in a broader magnetic-sweep range (50–550 mT), a broad tail emerged in the high field region (360–550 mT) together with a broad resonance signal in the low field region (around  $g = 4$ ) (ESI, Fig. S3†). These features became strongly weakened in the diluted systems (GrF/benzene and GrF/DMF). The ESI provides additional EPR spectra for GrF, including the EPR power-saturation behavior (Fig. S1a, S2–S4†). Panich and co-authors suggested that the fine structure observed around  $g = 2.00$  in GrF was due to resolved hyperfine components ( $A_F$ ) with  $\sim 5$  mT of splitting value, originating from the interaction of an unpaired spin ( $S = 1/2$ ) with six neighboring fluorine nuclei. The authors also

found that these hyperfine lines were rather broad ( $\Delta H = 30$  G by simulation), a factor that pointed towards the joint effect of dipole–dipole and exchange interactions between paramagnetic centers. In the later work, Giraudet and co-authors took the similar approach in the simulation of the observed EPR envelope for GrF, but with the addition of two broad resonance lines. The simulation of the signal was obtained by adding the hyperfine contribution of six fluorine nuclei ( $A = 45 \pm 2$  G, line width of  $36 \pm 2$  G, and  $g$  factor of  $2.003 \pm 0.001$ ). As stated by the authors, and similar to the Panich's work, “the large line width is interpreted by the joint effect of dipole–dipole and exchange interactions between paramagnetic centers”. In the case of the GrF/benzene frozen matrix sample, we therefore tried to disentangle these effects previously anticipated by ref. 41 and 42 and carried out an EPR simulation of the resonance signal in the  $g = 2.0$  region under the assumption of an overlapped contribution of different spin components (Fig. 1a, black line, Sim, and Fig. 1b showing the individual spin components with their relative weights). The observed EPR signal of GrF/benzene shown in Fig. 1a (Exp) can be interpreted as a superposition of three effective triplet states ( $S = 1$ ) and three sets of spin-doublets ( $S = 1/2$ ), *i.e.*, in GrF exists a distribution of spin-carrying defects, some close enough (through-space distance) to show signatures of high-spin systems and others behaving as isolated  $S = 1/2$  defects. This hypothesis is supported by the observation that the low field signal around  $g = 4.0$  observed in neat GrF can still be observed in the dilute



co-authors on the dominant spin-half paramagnetism for GrF-based materials.<sup>47</sup> Following GrF aging in benzene solution, we did not observe severe changes in the overall EPR resonance line, which remained after 6 days and 10 days similar to that shown at the beginning of the process (ESI, Fig. S8†). Thus, benzene can be considered a “nearly inert” solvent for GrF which does not induce substantial degradation of the paramagnetic centers. Chemical stability of GrF in benzene was also confirmed by measurement of the XPS spectrum for a 10-days aged GrF sample in benzene (Fig. S25 in ESI†). After dispersion of GrF in DMF, the freshly prepared suspension showed the same EPR fingerprints in a frozen matrix (Fig. 1c) as witnessed for GrF/benzene (Fig. 1a). Additional EPR spectra for GrF/DMF are given in the ESI† (power saturation behavior of the entire resonance line, from 50 to 550 mT, Fig. S9a–c†). The concentration of spin centers on the GrF surface at this stage was estimated to be  $23.2 \times 10^{18}$  spin per g, which corresponds to *ca.* 1 center per area of 5 nm  $\times$  5 nm (see ESI, section 1.2†). This value closely resembles the estimated spin concentration found to near stoichiometric C/F ratios in GrF (C/F<sub>0.9–1.0</sub>) by Grigorieva and co-authors, which were obtained from in-depth analysis of bulk magnetic susceptibility experiments ( $\sim 22\text{--}17 \times 10^{18}$  spin per g).<sup>47</sup> However, already after 6 h stirring at 40 °C, the GrF/DMF suspension darkened considerably. The X-band EPR spectrum ( $T = 123$  K) observed after 6 h revealed some changes in the overall resonance line (Fig. 1d) compared to the initial spectrum. The doublet component ( $S = 1/2$ ,  $D_1$  in the simulation shown in Fig. 1b) appeared to increase strongly in intensity (relative increase) at the expense of the  $T_1$ ,  $T_2$  and  $T_3$  triplet components (see  $S = 1$  components, Fig. 1b and ESI, Fig. S10†) and the doublet component  $D_2$ . After 7 days of stirring, the EPR spectrum of FG/DMF showed more significant changes (Fig. 1e). Besides still being centered at  $g_{\text{eff}} = 2.000$ , the doublet components  $D_1$  and  $D_2$  became dominant, several resonances appeared throughout the spectrum and a novel but very minor triplet emerged. The spin-Hamiltonian simulation of this species was very tentative (shown by the dotted red-line in Fig. 1e). This system should exhibit a large axial value ( $|D|$  of 1345 MHz,  $|E/D|$  of 0.04). In this case, the inter-spin (through-space) distance of the triplet configuration ( $S = 1$ , arising from two interacting  $S = 1/2$ ) was estimated from the point-dipole approach to fall short, at about 3.87 Å. This value corresponded well with the minimum through-space spin-spin distance of the spin carrying defects estimated by theory (*vide infra*, Fig. 4b). It is important to note that at such later stage of the GrF aging process, an alternative explanation for the appearance of the large triplet signal reported above can be put forward. Namely, it may arise from voids in the GrF sheets, especially in the areas corresponding to  $sp^2$  islands that are formed upon extended defluorination. As discussed by Palacios and co-authors,<sup>48</sup> the presence of voids, such as type A3B, can lead to non-vanishing local magnetic moments. Consequently,  $S = 1$  signatures can arise in the EPR spectrum from the presence of these sublattice imbalances ( $N_I = N_A - N_B$ ). When the Hubbard repulsion is active, Lieb’s theorem grants the  $S = 1$  spin state to such defect struc-



### 3.2 Origin of radical centers

EA, the extent of its delocalization increased with the system size. To sum up, although the energetically low-lying C-F  $\sigma^*$  orbital doubtlessly plays an important role in fluorine chemistry (*e.g.*, through orbital mixing, as explained by Borden applying the second-order perturbation theory<sup>56</sup>), it is improbable that mild reducing agents could initiate a radical cascade process of defluorination by direct electron transfer to the C-F  $\sigma^*$  orbital.

Although formation of radical centers on an ideal  $C_1F_1$  layer was expected to be hampered by the low EA, the experimental evidence of observable spin concentrations in  $C_1F_1$  structures clearly proves the presence of isolated  $sp^3$  carbon sites. The origin of such centers depends largely on the preparation process. Recent experimental surface imaging techniques have shown that fluorination of CVD graphene with  $XeF_2$  leads to formation of highly ordered sizable (150 nm) CF,  $C_2F$  chair and unfluorinated domains,<sup>60</sup> whereas fluorination with  $CF_4$  plasma gives rise to inhomogeneous and disordered microscopic configurations.<sup>61</sup> From a radical center formation point of view, in the former case, the carbon atoms at the boundary between these domains can remain unfluorinated as the attachment of fluorine on such sites would lead to a *cis* configurations, which would be energetically unfavorable.<sup>62</sup> On the other hand, the inhomogeneous spatial distribution of fluorine on CVD graphene treated with  $CF_4$  plasma is accompanied by formation of multilayer islands and structural features such as folds, wrinkles, and ripples that are less fluorinated, which consequently increases the probability of spin center emergence.

### 3.3 Electron affinities of radical centers

The presence of radical centers (even in very low concentrations) can obviously dramatically change the behavior of FG in the presence of reducing agents or nucleophilic species. As shown in Table S1 (see ESI<sup>†</sup>), the electron affinities of radical species derived from parent perfluorinated model systems are very high. For instance, AEA of a fluorinated coronene radical is 80.6 kcal mol<sup>-1</sup>, *i.e.*, it is even larger than that of a fluorine atom (78.4 kcal mol<sup>-1</sup>). These extremely large values of EA of perfluorinated radicals are mainly due to the electron-withdrawing effect of highly electronegative fluorine atoms bound to the nearest carbon atoms but also increased delocalization of the negative charge with increasing size of the system. This delocalization is closely related to the presence of the already discussed C-F  $\sigma^*$  orbitals on neighboring carbons, which can stabilize the SOMO orbital in a pyramidal configuration of the radical center by mutual orbital mixing.<sup>56,63</sup> The extraordinary oxidizing power of highly fluorinated organic radicals can initiate the defluorination process in the presence of even mild reducing agents. Therefore, we probed a possible scenario of initial phases of the cascade reduction of FG in which defluorination spreads outwards from a radical center (Fig. 2).

Although the total reaction enthalpies of the reduction steps depend on the strength of reducing agent as well as solvation enthalpies of the involved species, it can be seen that, in general, they are energetically favorable and polar solvents

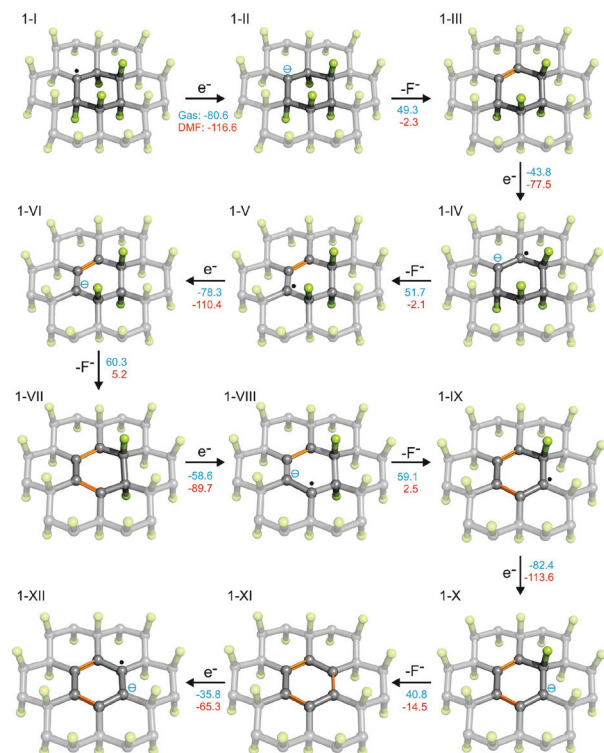


**Fig. 2** Possible scenario for the initial phases of reduction of FG (the F atoms in green, the C atoms in grey/black, newly formed C=C bonds in orange). The reaction energies are given in kcal mol<sup>-1</sup> (blue in gas phase and red in DMF).

stabilize the charged intermediates. As expected, the oxidizing power of the radical species is much higher (by about a factor of 2) than that of closed-shell systems occurring in the reduction process. However, even for the latter, the EA is rather high as a consequence of the effect of highly polar C-F bonds on the neighboring carbon atoms. Note that EA of the final structure **1-IX**, which is fully  $\pi$ -conjugated, is significantly lower than that of the other structures. It is therefore possible that depending on the power of the reducing agent, the cascade defluorination process may cease after formation of larger  $\pi$ -conjugated domains. Finally, let us consider possible formation of fluorine radicals by charge transfer from fluoride anions to the radical center. Although the gas phase value of the EA of **1-I** is slightly larger than that of an F atom, the stability of a small fluoride anion is significantly increased in polar solvents (much more than **1-II**), and therefore formation of F radicals by this mechanism would be unfavorable. Let us also underline that our results for model systems well reproduce those obtained for larger systems and are also in good correspondence with periodic calculations (see section 2.5 in ESI†).

### 3.4 Radical defluorination mechanism in DMF

We have shown that radical centers on FG act as efficient electron acceptors. Although such electron transfer can be a trigger for cascade defluorination, in the case of a sufficiently strong reducing agent, it does not explain the defluorination

of FG observed in solvents with ionization potential in the liquid phase significantly higher than the EA of FG point defects. An example of such a solvent is DMF (discussed in section 3.1), which has an ionization potential in the liquid phase of  $149 \text{ kcal mol}^{-1}$ , compared to the EA of a radical center **1-I** of  $117 \text{ kcal mol}^{-1}$  in the same solvent. Let us recall that electron affinities of the subsequent species are even smaller. Clearly, DMF can hardly be considered a direct reductant of FG in the sense of direct electron transfer to such radical centers.

To rationalize the observed spontaneous defluorination of FG in DMF, we suggest a mechanism initiated by hydrogen atom transfer from DMF to the FG radical center (Fig. 3). In

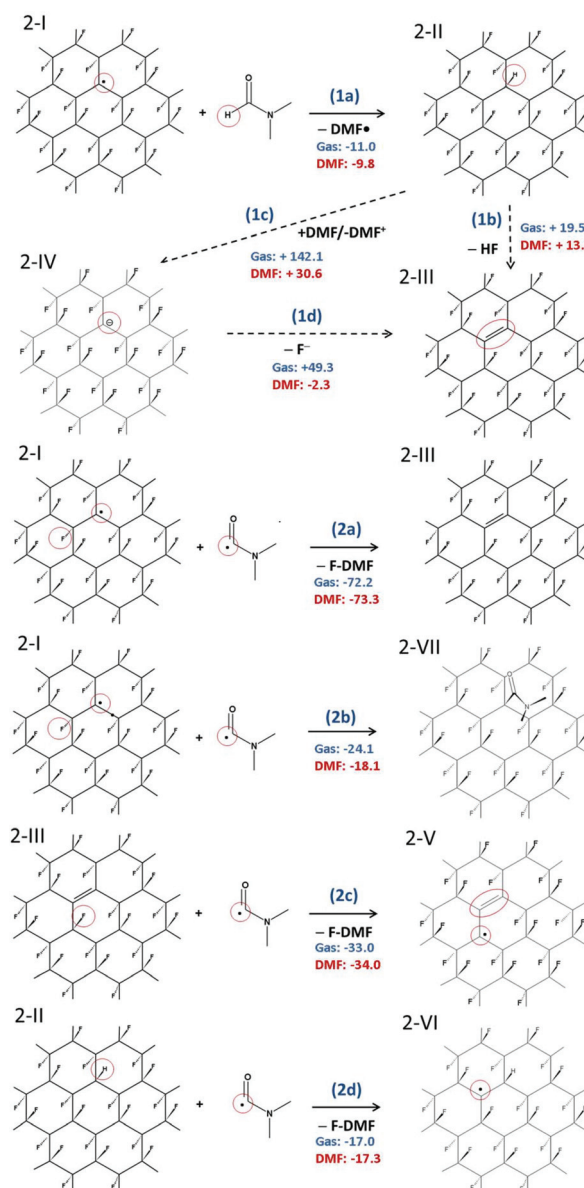
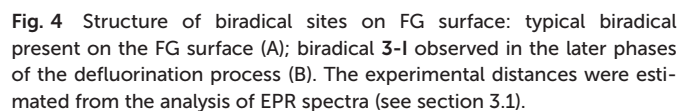
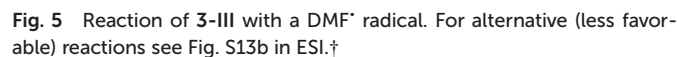


**Fig. 3** Radical mechanism of defluorination of FG in DMF. (1a–c) Initial phases of defluorination. (2a–d) Re-creation of FG radical center. The reaction energies are given in kcal mol<sup>-1</sup>.

As the EPR spectra of FG in DMF confirmed the presence of biradical centers (besides monoradical sites) on the FG surface, we also studied a radical mechanism of defluorination starting from structure **3-I** (Fig. 4), for which the theoretical distance between the spin centers (3.91 Å) was in reasonable



The same trapped radical species by POBN was obtained when the GrF/DMF solution was aged for a longer time (1 day, 7 days), whereas negative results were consistently found for a





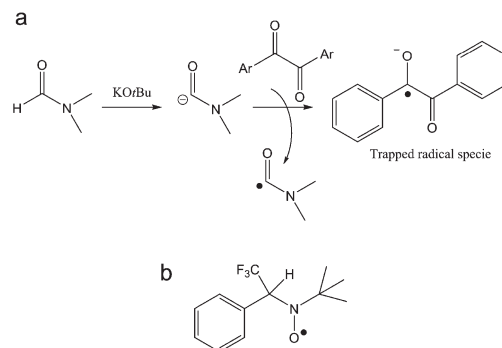


**Fig. 6** (a) Scheme for the reaction of  $\alpha$ -4-pyridyl-1-oxide-N-*tert*-butylnitrone (POBN) with free radicals to generate the corresponding spin-trapped nitroxide radical. (b) Chemical structure of a DMF<sup>•</sup> radical trapped by POBN. (c) X-band EPR spectra obtained from spin-trap (POBN) experiments carried out on the supernatant from a GrF/DMF/POBN mixture ( $T = 253$  K) together with its EPR simulation (red-trace), and (d) corresponding spectrum obtained in a frozen matrix ( $T = 133$  K) compared with simulation (red-trace). Experimental parameters: 9.16–9.17 GHz frequency, 100 kHz modulation frequency, 30 ms time constant, 0.2 mT (c) or 0.8 mT (d) modulation width, 0.3 mW (d) or 4.0 mW (c) applied microwave power. Simulation parameters are given in the text.

and  $A_H = 0.177$  mT, which the authors attributed to the successful entrapment of benzil anion radical by PBN (Fig. 7a, trapped radical species). Furthermore, Aggarwal *et al.*<sup>69</sup> recently reported the successful entrapment of a trifluoromethyl radical by PBN in DMF at 298 K (Fig. 7b), which exhibited  $g = 2.0044$ ,  $A_N = 1.411$  mT,  $A_H = 0.1664$  mT,  $A_F = 0.1781$  mT, hence, similar  $g_{iso}$ ,  $A_N$  and  $A_H$  as found for the GrF/DMF/POBN trapped radical system. Thus, because our system contains only GrF, and the POBN radical adducts can be trapped in DMF but not in benzene, the generation of the carbamoyl-radical trapped by POBN (POBN-DMF radical) as shown in Fig. 6b, is plausible.

The use of other experimental setups, *e.g.*, GrF sonication, as often employed for its fast dispersion in organic solvents, leads to generation of an admixture of radical species due to the fast temperature gradients induced in the solution. Due to the number of other experimental variables to dissect (*e.g.* sonication time, power applied) such study will be devoted for future work. As an example of other EPR signatures detected following the sequence of a specific sonication-time/applied power conditions (30 min, 40 kHz applied power) for the GrF/DMF/POBN mixture is given in the ESI (Fig. S20–S24†). However, the present findings wish to stress the notion that radical defluorination reactions of GrF occurs even under mild conditions in DMF.

As can be seen in Fig. 3, *N,N'*-dimethylcarbamoyl fluoride (F-DMF) plays a key role in the proposed mechanism since its formation leads directly to defluorination and also generation of new radical centers. To confirm formation of F-DMF, we performed a series of  $^{19}\text{F}$  NMR measurements on FG/DMF samples treated in different ways (see details in ESI†). The first sample was sonicated for 2 hours at room temperature and stirred overnight. The day after, the suspension was still pale-grey, the color of the starting suspension.  $^{19}\text{F}$  NMR analysis of the supernatant solution did not show the presence of any F-containing compounds. A second sample of FG/DMF was treated at 120 °C for 5 hours and then left stirring overnight at

room temperature. This time, the suspension appeared black, indicating that defluorination of FG had taken place. Using  $^{19}\text{F}$  NMR, the supernatant liquid showed the presence of one peak at  $-26$  ppm, which was attributed to F-DMF (Fig. 8a). Two more peaks, at  $-138$  and  $-152$  ppm, were also visible, which could be attributed to some soluble FG fragments (*cf.*,  $-135.85$ ,  $-162.45$  ppm for 1,2,3-trifluorobenzene, and  $-139.93$ ,  $-157.07$  ppm for 1,2,3,4-tetrafluorobenzene<sup>70</sup>) or to a product of reaction of fluoride ions with borosilicate glass (*cf.*,  $-152.2$  ppm for  $\text{BF}_4^-$  (ref. 71)). The peak at  $-26$  ppm was confirmed to be due to the F-DMF compound by separately preparing F-DMF,<sup>36,72</sup> whose  $^{19}\text{F}$  NMR spectrum in DMF also consisted of a peak at  $-26$  ppm (Fig. 8b). The stability of F-DMF under the experimental conditions was also assessed by adding an aliquot of the compound to a FG/DMF suspension heated at  $120^\circ\text{C}$  for 5 hours and then stirred overnight. In this case, the supernatant liquid showed again the presence of the compound peak at  $-26$  ppm (see ESI, Fig. S26†). Although it cannot be fully excluded that F-DMF can be produced by recombining  $\text{DMF}^\bullet$  and  $\text{F}^\bullet$  radicals (possibly formed during sonication process), the presence of the F-DMF peak in  $^{19}\text{F}$  NMR spectrum supports our hypothesis that defluorination of FG in DMF results from the direct reaction between  $\text{DMF}^\bullet$  and FG. The requirement of higher temperature indicates that steps (2a, 2c, 2d) in the proposed mechanism require some activation energy.

Finally, we will briefly comment on recent experimental work by Wang *et al.*,<sup>34</sup> in which defluorination of FG in the presence of selected solvents was studied by various instrumental techniques, including XRD, FTIR, TEM, TGA and UV-

vis reflectance spectroscopy. They found that highly polar (dipolar) solvents, including DMF, were able to facilitate the FG defluorination. They rationalized this capability in terms of high nucleophilicity, arguing that dipolar solvents can interact *via* dipole-dipole interactions with the electron-deficient carbon atom of a C-F bond, providing sufficient energy to rupture the C-F bond. To verify this hypothesis, we calculated the interaction energy of a DMF molecule with an ideal FG surface by using the implicit SMD model to account for the polar DMF environment (see ESI, Fig. S31†). Although the interaction energy was indeed found to be relatively high ( $4\text{ kcal mol}^{-1}$ ) compared to ordinary weakly interacting systems, it was still far below the dissociation energy of a C-F bond ( $\sim 100\text{ kcal mol}^{-1}$  for fluorinated coronene). Therefore, although we agree that the nucleophilicity of the solvent plays an important role in the later phases of defluorination, we believe that the proposed radical mechanism supported by the experimental evidence of the  $\text{DMF}^\bullet$  radical is a more plausible explanation of the initial steps of the FG defluorination process occurring in DMF.

### 3.7 Consequences for the reactivity of FG

We have shown that, depending on the chemical composition of the sample, the presence of radical centers on FG can initiate two important processes. On the one hand, direct reduction of FG (*i.e.*, formation of anionic centers) can occur in the presence of mild reducing agents. On the other hand, a radical mechanism initiated by hydrogen atom transfer can take place provided that species sensitive to homolytic R-H bond dissociation are present in the environment. In both cases, a cascade defluorination process can commence, leading preferentially to compact motifs stabilized by  $\pi$ -conjugation of C=C double bonds. It can be expected that the defluorinated chains of carbons carrying partial positive charge due to surrounding C-F bonds will be highly sensitive to nucleophilic substitutions. In fact, the idea of competitive substitution and reductive defluorination has already been applied to account for experimental observations during the covalent functionalization of graphene based on reactions of FG with various nucleophilic agents, including  $\text{OH}^-$ ,<sup>23</sup>  $\text{CN}^-$ ,<sup>31</sup> Grignard reagents<sup>33</sup> and others. In such reactions, the main indication of concurrent substitution and defluorination was

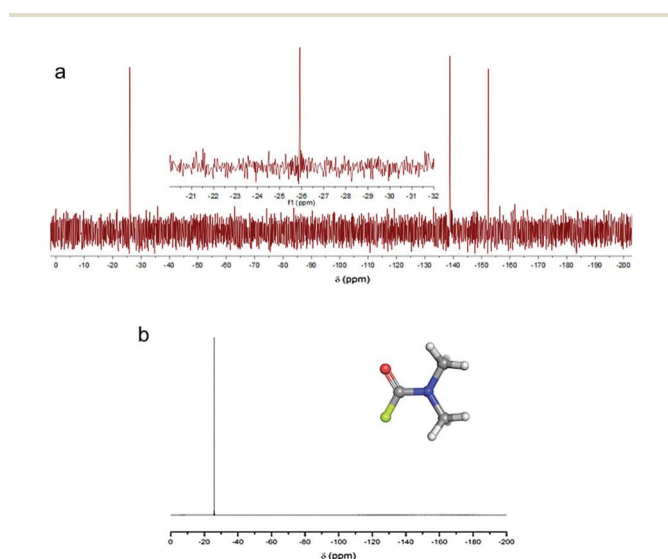


Fig. 8 (a)  $^{19}\text{F}$  NMR spectrum (in DMF, 470 MHz) of the supernatant liquid obtained from a FG/DMF suspension heated at  $120^\circ\text{C}$  for 5 hours and stirred at room temperature overnight (in the inset, a close-up of the peak at  $-26$  ppm is shown). (b)  $^{19}\text{F}$  NMR spectrum (in DMF, 470 MHz) of the separately prepared compound F-DMF (structure shown in inset). (b)  $^{19}\text{F}$  NMR spectrum (in DMF, 470 MHz) of the separately prepared compound F-DMF (structure shown in inset).

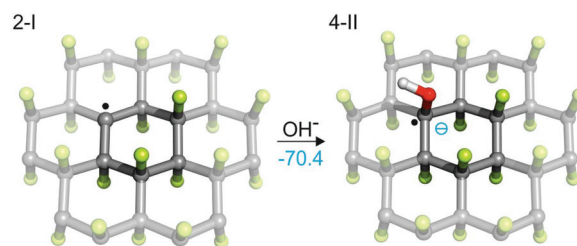


Fig. 9 Direct attack of a nucleophilic species (here  $\text{OH}^-$ ) on a radical site is energetically very favorable (energy in  $\text{kcal mol}^{-1}$  in the gas phase).



the composition of the resulting material, which showed only partial functionalization of graphene (e.g., ca. 15% in the case of G-CN) with negligible fluorine content. Nevertheless, the presence of radical centers in FG opens possibilities for direct attack of nucleophilic species on the radical site (Fig. 9). Such attacks could play an important role in the initiation of  $S_N$  reactions in solvents that are not able to trigger defluorination on their own (e.g., methanol, ethanol, chloroform). Our calculations showed that formation of a radical anion (**4-II**) is energetically highly favorable ( $\Delta E = -70.4 \text{ kcal mol}^{-1}$  for the gas phase), which strongly supports the idea that early-phase defluorination can be caused by direct interaction of a nucleophile with a radical center.

## Conclusions

Defluorination of FG is a complex process involving direct reduction, nucleophilic substitution or radical substitution reactions depending on the reductive and nucleophilic strengths of the solvent environment and/or presence of dissolved reactive agents. By combining DFT calculations with spectroscopic (EPR and NMR) studies, we have shown that it is the imperfectness of the FG sheets that induces its observed reactivity, distinguishing this 2D material from unreactive perfluorinated hydrocarbons, such as Teflon. The low-lying C-F  $\sigma^*$  orbitals in an ideal FG sheet could, in principle, render the structure susceptible to defluorination in the presence of strong reductants. However, it is improbable that mild reducing agents could initiate a cascade process of defluorination by direct electron transfer to the  $\sigma^*$  orbital. On the other hand, FG radical centers recorded by EPR measurements exhibit much higher electron affinities, making them ideal reactive sites for mild reducing agents and/or nucleophilic species. Nevertheless, even the relatively large electron acceptor strength of FG spin centers does not explain defluorination of FG in weakly reductive environments, such as DMF. In such cases, point defects can trigger a radical mechanism, provided that species sensitive to homolytic R-H bond dissociation are present in the environment. The proposed mechanism was supported by spin-trap experiments as well as  $^{19}\text{F}$  NMR measurements, which suggested formation of DMF $^{\bullet}$  radicals under mild reaction conditions (room temperature, simple stirring) and formation of F-DMF (under harsher conditions such as prolonged heating at 120 °C). To sum up, it is clear that point defects play a key role in the reactivity of FG. Understanding relationships between the reductive/nucleophilic strengths of the environment, possible formation of free radicals and point defect redox characteristics seems to be crucial for achieving full control over the functionalization of FG.

## Conflicts of interest

There are no conflicts to declare.

## Acknowledgements

We acknowledge financial support from the Ministry of Education, Youth and Sports of the Czech Republic (grants LO1305, CZ.1.05/2.1.00/19.0377 and the Research Infrastructure NanoEnvCz: project no. LM2015073), the ERC (Consolidator grant 683024 from the European Union's Horizon 2020 research and innovation programme), and the Neuron fund. We also thank Martin Petr for measuring the XPS spectra and Martin Pykal for preparing the TOC.

## References

- 1 K. S. Novoselov, A. K. Geim, S. V. Morozov, D. Jiang, Y. Zhang, S. V. Dubonos, I. V. Grigorieva and A. A. Firsov, *Science*, 2004, **306**, 666–669.
- 2 E. J. Duplock, M. Scheffler and P. J. D. Lindan, *Phys. Rev. Lett.*, 2004, **92**, 225502.
- 3 S. H. Cheng, K. Zou, F. Okino, H. R. Gutierrez, A. Gupta, N. Shen, P. C. Eklund, J. O. Sofo and J. Zhu, *Phys. Rev. B: Condens. Matter Mater. Phys.*, 2010, **81**, 205435.
- 4 D. C. Elias, R. R. Nair, T. M. G. Mohiuddin, S. V. Morozov, P. Blake, M. P. Halsall, A. C. Ferrari, D. W. Boukhvalov, M. I. Katsnelson, A. K. Geim and K. S. Novoselov, *Science*, 2009, **323**, 610–613.
- 5 L. G. Bulusheva, V. A. Tur, E. O. Fedorovskaya, I. P. Asanov, D. Pontiroli, M. Riccò and A. V. Okotrub, *Carbon*, 2014, **78**, 137–146.
- 6 A. Vizintin, M. Lozinsek, R. K. Chellappan, D. Foix, A. Krainc, G. Mali, G. Drazic, B. Genorio, R. Dedryvere and R. Dominko, *Chem. Mater.*, 2015, **27**, 7070–7081.
- 7 J. J. Xie, C. L. Li, Z. H. Cui and X. X. Guo, *Adv. Funct. Mater.*, 2015, **25**, 6519–6526.
- 8 V. Urbanova, F. Karlicky, A. Matej, F. Sembera, Z. Janousek, J. A. Perman, V. Ranc, K. Cepe, J. Michl, M. Otyepka and R. Zboril, *Nanoscale*, 2016, **8**, 12134–12142.
- 9 S.-Z. Liang, G. Chen, A. R. Harutyunyan, M. W. Cole and J. O. Sofo, *Appl. Phys. Lett.*, 2013, **103**, 233108.
- 10 S. Das, P. Sudhagar, V. Verma, D. Song, E. Ito, S. Y. Lee, Y. S. Kang and W. Choi, *Adv. Funct. Mater.*, 2011, **21**, 3729–3736.
- 11 L. Liao, H. L. Peng and Z. F. Liu, *J. Am. Chem. Soc.*, 2014, **136**, 12194–12200.
- 12 J. Park and M. D. Yan, *Acc. Chem. Res.*, 2013, **46**, 181–189.
- 13 S. P. Economopoulos, G. Rotas, Y. Miyata, H. Shinohara and N. Tagmatarchis, *ACS Nano*, 2010, **4**, 7499–7507.
- 14 J. M. Englert, C. Dotzer, G. A. Yang, M. Schmid, C. Papp, J. M. Gottfried, H. P. Steinruck, E. Spiecker, F. Hauke and A. Hirsch, *Nat. Chem.*, 2011, **3**, 279–286.
- 15 S. D. Bian, A. M. Scott, Y. Cao, Y. Liang, S. Osuna, K. N. Houk and A. B. Braunschweig, *J. Am. Chem. Soc.*, 2013, **135**, 9240–9243.
- 16 G. Dubey, R. Urcuyo, S. Abb, G. Rinke, M. Burghard, S. Rauschenbach and K. Kern, *J. Am. Chem. Soc.*, 2014, **136**, 13482–13485.





- 17 A. Y. S. Eng, C. K. Chua and M. Pumera, *Nanoscale*, 2015, **7**, 20256–20266.
- 18 S. Gilje, S. Han, M. Wang, K. L. Wang and R. B. Kaner, *Nano Lett.*, 2007, **7**, 3394–3398.
- 19 R. R. Nair, W. C. Ren, R. Jalil, I. Riaz, V. G. Kravets, L. Britnell, P. Blake, F. Schedin, A. S. Mayorov, S. J. Yuan, M. I. Katsnelson, H. M. Cheng, W. Strupinski, L. G. Bulusheva, A. V. Okotrub, I. V. Grigorieva, A. N. Grigorenko, K. S. Novoselov and A. K. Geim, *Small*, 2010, **6**, 2877–2884.
- 20 J. T. Robinson, J. S. Burgess, C. E. Junkermeier, S. C. Badescu, T. L. Reinecke, F. K. Perkins, M. K. Zalalutdniov, J. W. Baldwin, J. C. Culbertson, P. E. Sheehan and E. S. Snow, *Nano Lett.*, 2010, **10**, 3001–3005.
- 21 R. Zboril, F. Karlicky, A. B. Bourlinos, T. A. Steriotis, A. K. Stubos, V. Georgakilas, K. Safarova, D. Jancik, C. Trapalis and M. Otyepka, *Small*, 2010, **6**, 2885–2891.
- 22 K. A. Worsley, P. Ramesh, S. K. Mandal, S. Niyogi, M. E. Itkis and R. C. Haddon, *Chem. Phys. Lett.*, 2007, **445**, 51–56.
- 23 M. Dubecky, E. Otyepkova, P. Lazar, F. Karlicky, M. Petr, K. Cepe, P. Banas, R. Zboril and M. Otyepka, *J. Phys. Chem. Lett.*, 2015, **6**, 1430–1434.
- 24 P. Lazar, C. K. Chua, K. Hola, R. Zboril, M. Otyepka and M. Pumera, *Small*, 2015, **11**, 3790–3796.
- 25 V. Urbanova, K. Hola, A. B. Bourlinos, K. Cepe, A. Ambrosi, A. H. Loo, M. Pumera, F. Karlicky, M. Otyepka and R. Zboril, *Adv. Mater.*, 2015, **27**, 2305–2310.
- 26 K. E. Whitener, R. Stine, J. T. Robinson and P. E. Sheehan, *J. Phys. Chem. C*, 2015, **119**, 10507–10512.
- 27 R. Stine, J. W. Ciszek, D. E. Barlow, W. K. Lee, J. T. Robinson and P. E. Sheehan, *Langmuir*, 2012, **28**, 7957–7961.
- 28 C. Bosch-Navarro, M. Walker, N. R. Wilson and J. P. Rourke, *J. Mater. Chem. C*, 2015, **3**, 7627–7631.
- 29 B. Y. Li, T. J. He, Z. M. Wang, Z. Cheng, Y. Liu, T. Chen, W. C. Lai, X. Wang and X. Y. Liu, *Phys. Chem. Chem. Phys.*, 2016, **18**, 17495–17505.
- 30 X. Y. Ye, L. M. Ma, Z. G. Yang, J. Q. Wang, H. G. Wang and S. R. Yang, *ACS Appl. Mater. Interfaces*, 2016, **8**, 7483–7488.
- 31 A. Bakandritsos, M. Pykal, P. Blonski, P. Jakubec, D. D. Chronopoulos, K. Polakova, V. Georgakilas, K. Cepe, O. Tomanec, V. Ranc, A. B. Bourlinos, R. Zboril and M. Otyepka, *ACS Nano*, 2017, **11**, 2982–2991.
- 32 P. Kovaricek, Z. Bastl, V. Vales and M. Kalbac, *Chem. – Eur. J.*, 2016, **22**, 5404–5408.
- 33 D. D. Chronopoulos, A. Bakandritsos, P. Lazar, M. Pykal, K. Cepe, R. Zboril and M. Otyepka, *Chem. Mater.*, 2017, **29**, 926–930.
- 34 X. Wang, W. M. Wang, Y. Liu, M. M. Ren, H. N. Xiao and X. Y. Liu, *Phys. Chem. Chem. Phys.*, 2016, **18**, 3285–3293.
- 35 J. Tuček, K. Holá, A. B. Bourlinos, P. Błoński, A. Bakandritsos, J. Ugolotti, M. Dubecký, F. Karlický, V. Ranc, K. Čepe, M. Otyepka and R. Zbořil, *Nat. Commun.*, 2017, **8**, 14525.
- 36 J. Ichihara, T. Matsuo, T. Hanafusa and T. Ando, *J. Chem. Soc., Chem. Commun.*, 1986, 793–794.
- 37 J.-D. Chai and M. Head-Gordon, *Phys. Chem. Chem. Phys.*, 2008, **10**, 6615–6620.
- 38 R. Ditchfield, W. J. Hehre and J. A. Pople, *J. Chem. Phys.*, 1971, **54**, 724–728.
- 39 A. V. Marenich, C. J. Cramer and D. G. Truhlar, *J. Phys. Chem. B*, 2009, **113**, 6378–6396.
- 40 M. J. Frisch, G. W. Trucks, H. B. Schlegel, G. E. Scuseria, M. A. Robb, J. R. Cheeseman, G. Scalmani, V. Barone, B. Mennucci, G. A. Petersson, H. Nakatsuji, M. Caricato, X. Li, H. P. Hratchian, A. F. Izmaylov, J. Bloino, G. Zheng, J. L. Sonnenberg, M. Hada, M. Ehara, K. Toyota, R. Fukuda, J. Hasegawa, M. Ishida, T. Nakajima, Y. Honda, O. Kitao, H. Nakai, T. Vreven, J. A. Montgomery, J. E. Peralta, F. Ogliaro, M. Bearpark, J. J. Heyd, E. Brothers, K. N. Kudin, V. N. Staroverov, R. Kobayashi, J. Normand, K. Raghavachari, A. Rendell, J. C. Burant, S. S. Iyengar, J. Tomasi, M. Cossi, N. Rega, J. M. Millam, M. Klene, J. E. Knox, J. B. Cross, V. Bakken, C. Adamo, J. Jaramillo, R. Gomperts, R. E. Stratmann, O. Yazyev, A. J. Austin, R. Cammi, C. Pomelli, J. W. Ochterski, R. L. Martin, K. Morokuma, V. G. Zakrzewski, G. A. Voth, P. Salvador, J. J. Dannenberg, S. Dapprich, A. D. Daniels, O. Farkas, J. B. Foresman, J. V. Ortiz, J. Cioslowski and D. J. Fox, *Gaussian 09, Revision D.01*, Wallingford CT, 2009.
- 41 A. M. Panich, A. I. Shames and T. Nakajima, *J. Phys. Chem. Solids*, 2001, **62**, 959–964.
- 42 J. Giraudet, M. Dubois, A. Hamwi, W. E. E. Stone, P. Pirotte and F. Masin, *J. Phys. Chem. B*, 2005, **109**, 175–181.
- 43 R. Jain, M. B. Sponsler, F. D. Combs and D. A. Dougherty, *J. Am. Chem. Soc.*, 1988, **110**, 1356–1366.
- 44 C. Riplinger, J. P. Y. Kao, G. M. Rosen, V. Kathirvelu, G. R. Eaton, S. S. Eaton, A. Kutateladze and F. Neese, *J. Am. Chem. Soc.*, 2009, **131**, 10092–10106.
- 45 G. Zoppellaro, V. Enkelmann, A. Geies and M. Baumgarten, *Org. Lett.*, 2004, **6**, 4929–4932.
- 46 G. Zoppellaro, A. Geies, K. K. Andersson, V. Enkelmann and M. Baumgarten, *Eur. J. Org. Chem.*, 2008, 1431–1440.
- 47 R. R. Nair, M. Sepioni, I. L. Tsai, O. Lehtinen, J. Keinonen, A. V. Krashenninnikov, T. Thomson, A. K. Geim and I. V. Grigorieva, *Nat. Phys.*, 2012, **8**, 199–202.
- 48 J. J. Palacios, J. Fernández-Rossier and L. Brey, *Phys. Rev. B: Condens. Matter Mater. Phys.*, 2008, **77**, 195428.
- 49 E. H. Lieb, *Phys. Rev. Lett.*, 1989, **62**, 1201–1204.
- 50 J. Burdeniuc and R. H. Crabtree, *Science*, 1996, **271**, 340–341.
- 51 J. L. Kiplinger and T. G. Richmond, *Chem. Commun.*, 1996, 1115–1116.
- 52 J. L. Kiplinger and T. G. Richmond, *J. Am. Chem. Soc.*, 1996, **118**, 1805–1806.
- 53 J. Burdeniuc, P. E. M. Siegbahn and R. H. Crabtree, *New J. Chem.*, 1998, **22**, 503–510.
- 54 R. P. Hughes, T. LeHusebo, S. M. Maddock, A. L. Rheingold and I. A. Guzei, *J. Am. Chem. Soc.*, 1997, **119**, 10231–10232.
- 55 T. G. Richmond, *Angew. Chem., Int. Ed.*, 2000, **39**, 3241–3244.



- 56 W. T. Borden, *Chem. Commun.*, 1998, 1919–1925.
- 57 G. Sandford, *Tetrahedron*, 2003, **59**, 437–454.
- 58 F. Karlický and M. Otyepka, *J. Chem. Theory Comput.*, 2013, **9**, 4155–4164.
- 59 M. A. Ribas, A. K. Singh, P. B. Sorokin and B. I. Yakobson, *Nano Res.*, 2011, **4**, 143–152.
- 60 R. J. Kashtiban, M. A. Dyson, R. R. Nair, R. Zan, S. L. Wong, Q. Ramasse, A. K. Geim, U. Bangert and J. Sloan, *Nat. Commun.*, 2014, **5**, 4902.
- 61 B. Wang, J. J. Wang and J. Zhu, *ACS Nano*, 2014, **8**, 1862–1870.
- 62 A. M. Suarez, *Theory and Simulation of Atomic Hydrogen, Fluorine, and Oxygen on Graphene*, The Pennsylvania State University, 2012.
- 63 D. M. Lemal, *J. Org. Chem.*, 2004, **69**, 1–11.
- 64 W. Lai, D. Xu, X. Wang, Z. Wang, Y. Liu, X. Zhang, Y. Li and X. Liu, *Phys. Chem. Chem. Phys.*, 2017, **19**, 24076–24081.
- 65 D. K. Samarakoon, Z. Chen, C. Nicolas and X.-Q. Wang, *Small*, 2011, **7**, 965–969.
- 66 G. R. Buettner, *Free Radicals Biol. Med.*, 1987, **3**, 259–303.
- 67 G. M. K. Humphries and H. M. McConnell, Nitroxide Spin Labels, in *Methods in Experimental Physics*, ed. C. Marton, Academic Press, New York, 1982, vol. 20, pp. 53–122.
- 68 R. Ragno, A. Zaghi, G. Di Carmine, P. P. Giovannini, O. Bortolini, M. Fogagnolo, A. Molinari, A. Venturini and A. Massi, *Org. Biomol. Chem.*, 2016, **14**, 9823–9835.
- 69 Y. Wang, A. Noble, C. Sandford and V. K. Aggarwal, *Angew. Chem., Int. Ed.*, 2017, **56**, 1810–1814.
- 70 N. Y. Adonin, S. A. Prihod'ko, V. V. Bardin and V. N. Parmon, *Mendeleev Commun.*, 2009, **19**, 260–262.
- 71 H. Fenton, I. S. Tidmarsh and M. D. Ward, *Dalton Trans.*, 2009, 4199–4207.
- 72 R. P. Singh and J. n. M. Shreeve, *Chem. Commun.*, 2001, 1196–1197.

